Published in final edited form as:
Biomaterials. 2014 August ; 35(26): 7452–7459. doi:10.1016/j.biomaterials.2014.05.044.

The use of bi-layer silk fibroin scaffolds and small intestinal submucosa matrices to support bladder tissue regeneration in a rat model of spinal cord injury

Yeun Goo Chung[a,1], **Khalid Algarrahi**[a,1], **Debra Franck**[a], **Duong D. Tu**[a,b], **Rosalyn M. Adam**[a,b], **David L. Kaplan**[c], **Carlos R. Estrada Jr.**[a,b,**], and **Joshua R. Mauney**[a,b,*]

[a]Urological Diseases Research Center, Boston Children's Hospital, Boston, MA 02115, USA

[b]Department of Surgery, Harvard Medical School, Boston, MA 02115, USA

[c]Department of Biomedical Engineering, Tufts University, Medford, MA 02155, USA

Abstract

Adverse side-effects associated with enterocystoplasty for neurogenic bladder reconstruction have spawned the need for the development of alternative graft substitutes. Bi-layer silk fibroin (SF) scaffolds and small intestinal submucosa (SIS) matrices were investigated for their ability to support bladder tissue regeneration and function in a rat model of spinal cord injury (SCI). Bladder augmentation was performed with each scaffold configuration in SCI animals for 10 wk of implantation and compared to non-augmented control groups (normal and SCI alone). Animals subjected to SCI alone exhibited a 72% survival rate (13/18) while SCI rats receiving SIS and bi-layer SF scaffolds displayed respective survival rates of 83% (10/12) and 75% (9/12) over the course of the study period. Histological (Masson's trichrome analysis) and immunohistochemical (IHC) evaluations demonstrated both implant groups supported *de novo* formation of smooth muscle layers with contractile protein expression [α-smooth muscle actin (α-SMA) and SM22α] as well as maturation of multi-layer urothelia expressing cytokeratin (CK) and uroplakin 3A proteins. Histomorphometric analysis revealed bi-layer SF and SIS scaffolds respectively reconstituted 64% and 56% of the level of α-SMA+ smooth muscle bundles present in SCI-alone controls, while similar degrees of CK+ urothelium across all experimental groups were detected. Parallel evaluations showed similar degrees of vascular area and synaptophysin+ boutons in all regenerated tissues compared to SCI-alone controls. In addition, improvements in certain urodynamic parameters in SCI animals, such as decreased peak intravesical pressure, following implantation with both matrix configurations were also observed. The data presented in this study detail the ability of acellular SIS and bi-layer SF scaffolds to support formation of innervated, vascularized smooth muscle and urothelial tissues in a neurogenic bladder model.

*Corresponding author. Boston Children's Hospital, Department of Urology, John F. Enders Research Laboratories, 300 Longwood Ave., Rm. 1009, Boston, MA 02115, USA. Tel.: +1 617 919 2521; fax: +1 617 730 0248. joshua. mauney@childrens.harvard.edu (J.R. Mauney). **Corresponding author. Boston Children's Hospital, Department of Urology, 300 Longwood Ave., Hunnewell 3, Boston, MA 02115, USA. Tel.: +1 617 355 3338; fax: +1 617 730 0474. carlos.estrada@childrens.harvard.edu (C.R. Estrada).
[1]Equal contribution.

Keywords

Bladder tissue engineering; Small intestine submucosa; Silk; Urinary tract

1. Introduction

Spinal cord injury (SCI) and congenital neural tube defects such as myelomeningocele frequently disrupt voluntary control of micturition and lead to neurogenic bladder dysfunction [1]. In patients with a neurogenic bladder, disruption of normal neural pathways induces detrusor sphincter dyssynergia (DSD) causing urinary retention, a functional bladder outlet obstruction, and bladder overdistension [2,3]. This process results in extensive fibroproliferative tissue remodeling of the detrusor muscle which can ultimately lead to diminished bladder capacity and poor compliance [4,5]. Urologic complications secondary to spinal cord disorders including urinary incontinence, recurrent urinary tract infections and renal insufficiency or failure severely impact patient quality of life and contribute substantially to the clinical costs of disease management [6,7]. Standard treatment of the neurogenic bladder typically involves clean intermittent catheterization coupled with anti-cholinergic agents or botulinum toxin in order to mitigate the risk of renal damage from high pressure voiding and detrusor overactivity [8,9]. In cases where conservative therapies have failed, augmentation cystoplasty with autologous gastrointestinal segments represents the primary option for increasing bladder capacity and compliance in order to preserve upper urinary tract function [10]. However, this strategy is associated with substantial complications including metabolic abnormalities, chronic urinary tract infections, bowel dysfunction, and secondary malignancies [11,12].

Tissue engineering approaches utilizing biodegradable scaffolds either alone or seeded with primary cell sources have been explored as alternatives to enterocystoplasty for management of neurogenic bladder dysfunction in both animal models [13–15] and clinical trials [16,17]. In particular, decellularized collagen-based bladder acellular matrix (BAM) has been previously utilized as an acellular graft for bladder augmentation in a rat model of spinal cord injury [13–15]. In these reports, BAM was capable of promoting regeneration of innervated, vascularized smooth muscle and urothelial tissues within implantation sites by supporting host tissue integration [13–15]. Improvements in urodynamic parameters such as bladder capacity and compliance were also evident in SCI animals following BAM grafting [14,15]. Overall, the ability of BAM to encourage functional tissue regeneration within the setting of a neurogenic bladder was found to be comparable to the results observed in healthy animals [14]. Nonetheless, substantial adverse effects including atrophy of grafted BAM, pyuria, implant contracture, urinary tract infections, and urinary calculi were still observed in the augmented SCI model [13,14] raising concerns over the translational potential of this biomaterial for clinical deployment.

Short-term clinical trials reported by Atala and colleagues first demonstrated the ability of a collagen-coated poly-glycolic acid mesh, seeded with patient-derived smooth muscle and urothelial cells expanded *ex vivo*, to mediate *de novo* bladder tissue formation in children with myelomeningocele [16]. However, phase II studies of this technology at 3 years post-implantation failed to show significant improvements in bladder capacity or compliance

within the neurogenic bladder population [17]. In addition, the level of serious adverse events including bowel obstruction and bladder rupture encountered with this approach were reported to surpass an acceptable safety standard [17]. Therefore, there exists a substantial need for the development of novel methods for bladder reconstruction in patients with spinal cord defects.

We hypothesized that an optimal strategy for augmentation cystoplasty of the neurogenic bladder would consist of an “off-the-shelf” acellular graft with the structural, mechanical, and degradation properties sufficient to support initial defect stabilization while allowing for gradual remodeling, host tissue ingrowth, and subsequent tissue regeneration without adverse immunogenic reactions. Bi-layer silk fibroin (SF) scaffolds derived from *Bombyx mori* silkworm cocoons as well as porcine small intestinal submucosa have been previously shown to promote defect consolidation and mediate functional voiding in non-diseased animal models of bladder augmentation [18–24]. These matrices, therefore, represent potential candidates for neurogenic bladder repair; however their performance in the setting of neuropathogenic disease is currently unknown. In the present study, we investigated the efficacy of these scaffolds to support tissue regeneration and bladder function in a rat model of SCI.

2. Materials and methods

2.1. Biomaterials

Aqueous SF solutions were prepared from *B. mori* silkworm cocoons using published procedures [25] and utilized to construct a bi-layer SF matrix using methods previously described [24]. Briefly, an SF solution (8% wt/vol) was poured into a rectangular casting vessel and dried in a laminar flow hood at room temperature for 48 h to achieve formation of an SF film. A 6% wt/vol SF solution was then mixed with sieved granular NaCl (500–600 μM, average crystal size) in a ratio of 2 g NaCl per ml of SF solution and layered on to the surface of the SF film. The resultant solution was allowed to cast and fuse to the SF film for 48 h at 37 °C and NaCl was subsequently removed by washing the scaffold for 72 h in distilled water with regular volume changes. The morphology of the bi-layer SF scaffold has been previously reported [24]. Briefly, the solvent-cast/NaCl-leached layer comprised the bulk of the total matrix thickness (2 mm) and resembled a foam configuration with large pores (pore size, ~400 μm) interconnected by a network of smaller pores dispersed along their periphery. This compartment was buttressed on the external face with a homogenous, non-porous SF layer (200 μm thick) generated by film annealment during casting. Before implantation, bi-layer SF scaffolds were sterilized in 70% ethanol and rinsed in phosphate buffered saline (PBS) overnight. SIS grafts (Cook, Bloomington, IN) were evaluated in parallel. Tensile properties of both scaffold configurations have been previously reported [24].

2.2. SCI model and bladder augmentation

Forty-two female Sprague–Dawley rats (6 wk of age, Charles River Laboratories, Wilmington, MA) were subjected to complete extradural spinal cord transection at the 8th thoracic level (T8) to elicit a previously described reflex bladder phenotype with

overactivity [26]. This model has been reported to produce spinal cord lesions containing glial scarring as well as neuronal damage, consisting of neuronal swelling and chromatin dispersion with focal chromatolysis [26]. Under general anesthesia induced by isoflurane inhalation, a dorsal midline incision was made through the superficial and deep muscle layers over the thoracic spinal cord. Posterior laminectomy was executed and a dorsal transection across the entire width of the spinal cord at T8 was performed with a scalpel blade. Excision of 2–3 mm of spinal cord tissue was carried out to ensure complete transection and the subsequent gap was filled with absorbable gelatin sponge (Ethicon™). Muscle and skin layers were subsequently closed with absorbable sutures. Post-operative pain was managed with meloxicam (1 mg/kg, subcutaneously) analgesia. During the period of spinal shock, which lasted from 1 to 3 wk following creation of SCI, bladders of rats were emptied twice daily by manual compression with care taken to avoid unintentional bladder rupture.

Following 6 wk of SCI, 24 animals were divided into 2 groups of 12 and subjected to augmentation cystoplasty with either SIS (Group 1, SCI–SIS) or bi-layer SF scaffolds (Group 2, SCI–SF) for 10 wk of implantation as previously described [24,27]. The 14 remaining SCI animals were maintained similarly in parallel as longitudinal controls without matrix grafting (Group 3, SCI-control). For bladder augmentation studies, animals were anesthetized using isoflurane inhalation and then shaved to expose the surgical site. A low midline laparotomy incision was then made and the underlying tissue (rectus muscle and peritoneum) was dissected free to expose the bladder. Four traction sutures (7-0 polypropylene) were placed in a square configuration. A longitudinal cystotomy incision was then made in the bladder dome in the middle of these traction sutures using fine scissors to create a bladder defect (Fig. 1A). A circular piece of biomaterial (~10 mm in diameter) was then anastamosed to this site using 7-0 vicryl continuous suture (Fig. 1B). Non-absorbable 7-0 polypropylene sutures were placed at the edges of the implantation area for identification of graft borders. A watertight seal was confirmed by filling the bladder with sterile saline via instillation through a 30 gauge hypodermic needle. Skin incisions were subsequently closed with running sutures. At 10 wk post-augmentation, animals were harvested for endpoint evaluations described below. In addition, 11 normal rats not receiving bladder implants (Group 4, NS-Control) were analyzed in parallel as a positive control cohort. All animal studies were approved by the Boston Children’s Hospital Animal Care and Use Committee prior to experimentation.

2.3. Cystometric analyses

Bladder urodynamics were evaluated in all experimental groups using conscious unrestrained cystometry previously described [24,26,27]. A suprapubic (SP) catheter was surgically inserted into the bladder 1–3 d prior to cystometry. Under isoflurane anesthesia, a laparotomy was created using a ventral lower midline incision. A flared tip SP catheter (polyethylene-50; Intramedic, Sparks, MD) was inserted into the bladder, secured with 6-0 prolene purse-string suture, and tunneled through the subcutaneous area to a dorsal midline skin incision between the scapulae. An access port was connected to the outlet of the SP catheter on the dorsal aspect with a luer-lock inter-link system (Injection site; Baxter, Deerfield, IL).

During cystometry, the SP catheter was attached to a physiological pressure transducer (model MLT844, ADInstruments, Colorado Springs, CO) to allow measurement of intravesical pressure, while the bladder was continuously infused with sterile PBS at 100 μl/min. Pressure readings were digitized using a PowerLab data acquisition system and analyzed using LabChart Pro software (ADInstruments, Colorado Springs, CO). Post void residual volumes were measured by aspirating the SP catheter at the conclusion of cystometry. After establishment of a regular voiding pattern, multiple other variables were extrapolated from the cystometric tracings, such as compliance, spontaneous non-voiding contractions (SNVC), resting pressure, voided volume, peak intravesical pressure, start filling pressure, end filling pressure, and bladder capacity. SNVC were defined as any bladder activity wherein intravesical pressure of >5 cm H_2O was achieved without voiding. Compliance was calculated by dividing the change of bladder volume by the change of intravesical pressure during the first filling phase. A total of 5–6 animals per group with 4 consecutive micturition cycles per animal were analyzed to determine urodynamic parameters.

2.4. Histological, immunohistochemical, and histomorphometric analyses

Following scheduled euthanasia, bladders were excised for standard histological processing. Briefly, bladders were weighed and fixed in 10% neutral-buffered formalin, dehydrated in graded alcohols, and then embedded in paraffin. Sections (5 μm) were cut and then stained with hematoxylin and eosin (H&E) or Masson's trichrome (MTS) using routine histological protocols. For immunohistochemical (IHC) analyses, contractile smooth muscle markers such as α-smooth muscle actin (α-SMA) and SM22α; urothelial-associated proteins, cytokeratins (CK) and uroplakin (UP) 3A; neuronal and endothelial markers, synaptophysin (SYP38) and CD31, respectively, were detected using the following primary antibodies: anti-α-SMA [Sigma–Aldrich, St. Louis, MO, 1:200 dilution], anti-SM22α [Abcam, Cambridge, MA, 1:200 dilution], anti-pan-CK [Dako, Carpinteria, CA, 1:200 dilution], anti-UP3A [Fitzgerald Industries, Acton, MA, 1:200 dilution], anti-SYP38 [Abcam, 1:200 dilution], anti-CD31 [Abcam,1:100 dilution]. Sections were then incubated with species-matched Cy3-conjugated secondary antibodies (Millipore, Billerica, MA) and nuclei were counterstained with 4′,6-diamidino-2-phenyllindole (DAPI). Specimens were visualized using an Axioplan-2 microscope (Carl Zeiss MicroImaging, Thornwood, NY) and representative images were acquired using Axiovision software (version 4.8).

Histomorphometric analysis (N = 4–5 animals per group) was performed as previously described [28] to assess the degree of smooth muscle and urothelial tissue regeneration in both control and implant groups using ImageJ software (version 1.47). Image thresholding and area measurements were carried out on 8 independent microscopic fields (magnification 20×) equally dispersed along the periphery and central regions of the original surgical sites to determine the percentage of tissue area occupied by α-SMA+ smooth muscle bundles and CK+ urothelium relative to the total tissue area examined. The number and diameter of CD31+ vessels and SYP38+ boutons were measured similarly in 4 independent microscopic fields (magnification 20×) and normalized to the total tissue area examined to ascertain the respective extent of *de novo* vascularization and innervation processes in all experimental

groups. Vascular area was calculated by multiplying the total vessel number by the mean vessel diameter.

2.5. Statistical analysis

Quantitative measurements for urodynamic and histomorphometric parameters were analyzed with the Kruskal–Wallis test in combination with the post-hoc Scheffé 's method. Bladder-to-body weight ratios were analyzed with the Man-n–Whitney *U* test. All statistical evaluations were performed with SPSS Statistics software v19.0 (http://www.spss.com) and all data were expressed as means ± standard deviation. Statistically significant values were defined as $p < 0.05$.

3. Results and discussion

Animals subjected to SCI alone exhibited a 72% survival rate (13/18) with 5 deaths occurring as a result of spontaneous bladder rupture between 4 and 50 d post-op. Over the course of the 10 wk implantation period, SCI rats receiving SIS and bi-layer SF scaffolds displayed respective survival rates of 83% (10/12) and 75% (9/12). Animal mortality in both scaffold groups occurred within the first wk and post-mortem analysis revealed urinary ascites as the probable cause of death due to urine leak. In comparison to our previous studies in normal rats [24], bladder augmentation with SIS and bi-layer SF scaffolds in SCI animals resulted in a 5% and 25%, respective, increase in the incidence of animal death, however survival rates for both matrix groups were still higher than those observed in animals receiving SCI alone demonstrating minimal impact of scaffold grafting on this parameter.

Following scheduled euthanasia, gross tissue evaluations of the lower urinary tract revealed no signs of bladder mucus or hydronephrosis in any of the sacrificed animals. Consistent with previous reports in the literature [26,29], the bladder-to-body weight ratios in animals receiving SCI alone (Group 3; 0.0024 ± 0.0015) were significantly higher (3.7× $p < 0.05$) in comparison to normal controls (Group 4; 0.00065 ± 00017), as a result of increased bladder weights following SCI. In contrast to Groups 3–4, SCI rats receiving SIS and bi-layer SF implants displayed the presence of luminal bladder stones with a respective frequency of 55% (5/9) and 66% (6/9). The incidence of stone formation was substantially higher in SCI animals grafted with bi-layer SF scaffolds in comparison to our previous studies in non-diseased cohorts where the observed frequency was 20% [24]. In contrast, the frequency of stone formation following SIS implantation in normal rats (57%) [24] was similar to the level observed in this study. Urinary calculi are a common occurrence in rat models of bladder augmentation with biodegradable scaffolds wherein accumulation of residual matrix fragments within the bladder lumen can serve as a nidus for stone formation [30,31]. Indeed, we routinely observed remnants of both scaffold configurations within the interior of intravesical stones present in SCI animals. Increasing the in vivo degradation rate of bi-layer SF scaffolds through pre-treatment with proteolytic enzymes [32] prior to implantation may serve as a useful strategy to minimize residual matrix fragments and reduce urinary stone formation.

Gross tissue evaluations of augmented bladders in both Groups 1 and 2 following 10 wk of biomaterial incorporation demonstrated extensive host tissue ingrowth which spanned the entire area of the original implantation site with negligible contraction observed between the marking sutures (Fig. 1C, D). Global histological analyses (MTS) of the *de novo* bladder wall supported by both bi-layer SF and SIS scaffolds demonstrated cross-sectional organization with distinct compartments consisting of a luminal, multi-layer urothelium, an extra-cellular matrix (ECM)-rich lamina propria, and an outer layer of smooth muscle bundles which resembled the tissue architecture of Groups 3 and 4 (Fig. 2). However, in contrast to the non-augmented control groups, varying degrees of urothelial hyperplasia were observed within the regenerated tissues supported by both scaffold configurations; features which mimicked our previous observations of bladder tissue regeneration in normal animals [24].

Over the course of the 10 wk implantation period, SIS and bi-layer SF scaffolds underwent extensive degradation wherein residual remnants of both matrix types were noted within the bladder lumen (Fig. 3A, B) while the *de novo* bladder wall also contained pockets of highly fragmented portions of the bi-layer SF scaffold (Fig. 3C). Discrete areas of mild fibrosis within the lamina propria of the consolidated tissues supported by each matrix configuration were also detected (data not shown). H&E analysis of Groups 1 and 2 demonstrated the presence of chronic inflammatory reactions within the regenerated tissues characterized by mobilized follicular aggregates of mononuclear cell infiltrates (Fig. 3D, E). These results are in contrast to our previous observations in a non-diseased rat model where no chronic inflammatory events were observed following augmentation cystoplasty with these scaffold configurations [24]. In addition, eosinophil granulocytes indicative of minimal acute inflammatory reactions were also present in the *de novo* bladder wall supported by the bi-layer SF matrix (Fig. 3F), but were not observed in response to SIS implantation.

IHC evaluations (Fig. 4A) revealed α-SMA and SM22α contractile protein expression in the smooth muscle layers supported by all experimental groups indicative of smooth muscle differentiation. Histomorphometric analysis (Fig. 4A′) revealed statistically similar degrees of α-SMA+ smooth muscle bundles in both control groups reflecting minimal impact of SCI on this parameter. However, the number of *de novo* α-SMA+ smooth muscle bundles supported by bi-layer SF and SIS matrices was significantly lower in comparison to non-augmented SCI animals reaching only 64% and 56% of control levels, respectively. A previous study by Sharma and colleagues demonstrated that cell seeding of synthetic elastomeric scaffolds with bone marrow-derived stem cell populations from spina bifida patients enhanced the extent of smooth muscle tissue formation over acellular matrices in a non-diseased rodent model of bladder augmentation [33]. This approach may represent a useful strategy to improve the propensity of bi-layer SF and SIS scaffolds to promote smooth muscle regeneration in the setting of SCI. In addition, urothelial maturation within the *de novo* bladder walls supported by each matrix configuration was evidenced by prominent CK and UP3A expression (Fig. 4B). Histomorphometric analysis (Fig. 4B′) demonstrated statistically similar degrees of CK+ urothelium across all experimental groups. These results highlight the ability of both acellular bi-layer SF and SIS scaffolds to support re-epithelialization of the original defect sites in bladders of SCI animals.

As a result of SCI, a significant reduction in the density of SYP38+ boutons within the neurogenic bladder wall was observed in comparison to NS-controls indicating pathological remodeling of normal synaptic transmission areas (Fig. 4C, C′). Following 10 wk of implantation with bi-layer SF and SIS scaffolds, reconstituted tissues in both groups displayed statistically similar densities of SYP38+ boutons as seen in non-augmented SCI controls, however these levels were still significantly lower than those observed in the non-injured cohort. These data suggest that acellular scaffolds can support the formation of *de novo* innervation processes within implantation sites; however restoration of normal neuronal circuitry during defect consolidation is limited by the neurogenic bladder environment.

Regenerated tissues mediated by both bi-layer SF and SIS matrices displayed evidence of *de novo* vascularization throughout the original implantation sites indicated by the appearance of vessels containing CD31+ endothelial cells (Fig. 4D). However, histomorphometric evaluations (Fig. 4D′) demonstrated that the vascularization pattern was differentially affected by the type of matrix configuration used for bladder augmentation. In comparison to SCI controls, the density and mean diameter of CD31+ vessels promoted by the SCI–SF group was statistically similar revealing that bi-layer SF scaffolds could support restoration of the original vascular pattern of the neurogenic bladder wall. In contrast, SIS implantation led to a significant increase in the density of CD31+ vessels with a corresponding significant decrease in mean vessel diameter in respect to SCI controls. Vascular area, which is dependent on vessel density and diameter, was found to be statistically similar across all experimental groups (NS-control, 1.2 ± 0.7 mm^2; SCI-control, 1.3 ± 0.5 mm^2; SCI–SF, 1.5 ± 0.3 mm^2; SCI–SIS, 0.7 ± 0.2 mm^2). Vascular area is a potentially more descriptive indicator of the extent of construct vascularization than vessel density and diameter alone [34]. Therefore our results imply that both implant groups could reconstitute the level of bladder wall vascularization present prior to augmentation.

Previous reports of SCI in rats have shown that suprasacral spinalization produces an initial period of bladder areflexia that lasts for several days which is frequently followed by the development of a hyper-reflexic phenotype characterized by an increase in SNVC [14,26]. In the current study, cystometric evaluations (Table 1) of non-augmented animals following 16 wk of SCI revealed significant elevations in SNVC and peak intravesical and resting pressures in comparison to normal controls. In addition, significantly higher start and end filling pressures were observed in SCI rats relative to those in the non-diseased cohort, which were accompanied by significant elevations in post-void residual volumes. Alterations in these urodynamic parameters were presumably due to DSD elicited by SCI which is known to cause incomplete emptying and high pressure voiding [2].

Bladder augmentation with SIS and bi-layer SF scaffolds led to significant reductions in peak intravesical pressure in comparison to respective SCI controls. Implantation of SIS matrices also significantly attenuated resting as well as start and end filling pressures in relation to SCI-control levels. These results are in contrast to bi-layer SF scaffolds which did not significantly impact these measurements. Despite evidence of *de novo* tissue formation following SIS and bi-layer SF matrix implantation, no significant increases in bladder capacity or voided volumes in respect to non-augmented SCI controls were observed in our

analyses. These observations may be explained by the high frequency of intravesical stones present in these groups which may have masked volumetric gains in these parameters. Bladder compliance was also not significantly improved in SCI animals receiving either matrix configuration over respective SCI controls. These results are in contrast to our previous bladder augmentation studies in non-diseased rats wherein bi-layer SF scaffolds were capable of increasing organ compliance [24]. Differences between the mechanical properties of the regenerated bladder walls formed in normal and neurogenic disease settings may account for this discrepancy, however further investigation is warranted to confirm this notion. In addition, the lack of significant reductions in post-void residual volumes or SNVC following neurogenic bladder augmentation suggests that combinatorial management with anti-cholinergics [17] may still be required to treat these symptoms.

4. Conclusions

The data presented in this report detail the ability of acellular SIS and bi-layer SF scaffolds to support formation of innervated, vascularized smooth muscle and urothelial tissues in a neurogenic bladder model. Improvements in certain urodynamic parameters in SCI animals, such as decreased peak intravesical pressure, following implantation with both matrix configurations provides indications that these biomaterials may be useful in mitigating the risk of upper urinary tract damage in cases where high pressure voiding is encountered. In comparison to SIS matrices, modulation of the structural, mechanical, and degradation properties of bi-layer SF scaffolds through manipulation of scaffold processing parameters may offer more flexibility in optimizing next generation prototypes capable of reducing the incidence of stone formation and increasing organ compliance. In summary, acellular scaffolds derived from small intestinal submucosa and silk fibroin offer promising platforms for neurogenic bladder augmentation.

Acknowledgments

Xuehui Yang is acknowledged for her technical assistance with tissue processing for histological analyses. This research was supported by the Tissue Engineering Resource Center, NIH/NIBIB P41 EB002520 (KAPLAN); NIH/NIDDK P50 DK065298 (ADAM); NIH/NIDDK T32-DK60442 (FREEMAN); NIH/NIDDK R00 DK083616-01A2 (MAUNEY).

References

1. Ginsberg D. The epidemiology and pathophysiology of neurogenic bladder. Am J Manag Care. 2013; 19:s191–6. [PubMed: 24495240]
2. Kaplan SA, Chancellor MB, Blaivas JG. Bladder and sphincter behavior in patients with spinal cord lesions. J Urol. 1991; 146:113–7. [PubMed: 2056568]
3. Dorsher PT, McIntosh PM. Neurogenic bladder. Adv Urol. 2012; 2012:816274. [PubMed: 22400020]
4. Landau EH, Jayanthi VR, Churchill BM, Shapiro E, Gilmour RF, Khoury AE, et al. Loss of elasticity in dysfunctional bladders: urodynamic and histochemical correlation. J Urol. 1994; 152:702–5. [PubMed: 8021999]
5. Compérat E, Reitz A, Delcourt A, Capron F, Denys P, Chartier-Kastler E. Histologic features in the urinary bladder wall affected from neurogenic overactivity-a comparison of inflammation, oedema and fibrosis with and without injection of botulinum toxin type A. Eur Urol. 2006; 50:1058–64. [PubMed: 16517054]

6. Anderson KD. Targeting recovery: priorities of the spinal cord-injured population. J Neurotrauma. 2004; 21:1371–83. [PubMed: 15672628]
7. Krueger H, Noonan VK, Trenaman LM, Joshi P, Rivers CS. The economic burden of traumatic spinal cord injury in Canada. Chronic Dis Inj Can. 2013; 33:113–22. [PubMed: 23735450]
8. Larijani FJ, Moghtaderi M, Hajizadeh N, Assadi F. Preventing kidney injury in children with neurogenic bladder dysfunction. Int J Prev Med. 2013; 4:1359–64. [PubMed: 24498490]
9. Soljanik I. Efficacy and safety of botulinum toxin A intradetrusor injections in adults with neurogenic detrusor overactivity/neurogenic overactive bladder: a systematic review. Drugs. 2013; 73:1055–66. [PubMed: 23775527]
10. Guys JM, Hery G, Haddad M, Borrionne C. Neurogenic bladder in children: basic principles, new therapeutic trends. Scand J Surg. 2011; 100:256–63. [PubMed: 22182847]
11. Scales CD Jr, Wiener JS. Evaluating outcomes of enterocystoplasty in patients with spina bifida: a review of the literature. J Urol. 2008; 180:2323–9. [PubMed: 18930285]
12. Husmann DA, Rathbun SR. Long-term follow up of enteric bladder augmentations: the risk for malignancy. J Pediatr Urol. 2008; 4:381–5. [PubMed: 18653384]
13. Obara T, Matsuura S, Narita S, Satoh S, Tsuchiya N, Habuchi T. Bladder acellular matrix grafting regenerates urinary bladder in the spinal cord injury rat. Urology. 2006; 68:892–7. [PubMed: 17070388]
14. Urakami S, Shiina H, Enokida H, Kawamoto K, Kikuno N, Fandel T, et al. Functional improvement in spinal cord injury-induced neurogenic bladder by bladder augmentation using bladder acellular matrix graft in the rat. World J Urol. 2007; 25:207–13. [PubMed: 17221271]
15. Kikuno N, Kawamoto K, Hirata H, Vejdani K, Kawakami K, Fandel T, et al. Nerve growth factor combined with vascular endothelial growth factor enhances regeneration of bladder acellular matrix graft in spinal cord injury-induced neurogenic rat bladder. BJU Int. 2009; 103:1424–8. [PubMed: 18990142]
16. Atala A, Bauer SB, Soker S, Yoo JJ, Retik AB. Tissue-engineered autologous bladders for patients needing cystoplasty. Lancet. 2006; 367:1241–6. [PubMed: 16631879]
17. Joseph DB, Borer JG, De Filippo RE, Hodges SJ, McLorie GA. Autologous cell seeded biodegradable scaffold for augmentation cystoplasty: phase ii study in children and adolescents with spina bifida. J Urol. 2014; 191:1389–95. [PubMed: 24184366]
18. Kropp BP, Rippy MK, Badylak SF, Adams MC, Keating MA, Rink RC, et al. Regenerative urinary bladder augmentation using small intestinal submucosa: urodynamic and histopathologic assessment in long-term canine bladder augmentations. J Urol. 1996; 155:2098–104. [PubMed: 8618344]
19. Kropp BP. Small-intestinal submucosa for bladder augmentation: a review of preclinical studies. World J Urol. 1998; 16:262–7. [PubMed: 9775425]
20. Kropp BP, Cheng EY, Lin HK, Zhang Y. Reliable and reproducible bladder regeneration using unseeded distal small intestinal submucosa. J Urol. 2004; 172:1710–3. [PubMed: 15371796]
21. Mauney JR, Cannon GM, Lovett ML, Gong EM, Di Vizio D, Gomez P 3rd, et al. Evaluation of gel spun silk-based biomaterials in a murine model of bladder augmentation. Biomaterials. 2011; 32:808–18. [PubMed: 20951426]
22. Gomez P 3rd, Gil ES, Lovett ML, Rockwood DN, Di Vizio D, Kaplan DL, et al. The effect of manipulation of silk scaffold fabrication parameters on matrix performance in a murine model of bladder augmentation. Biomaterials. 2011; 32:7562–70. [PubMed: 21764119]
23. Tu DD, Chung YG, Gil ES, Seth A, Franck D, Cristofaro V, et al. Bladder tissue regeneration using acellular bi-layer silk scaffolds in a large animal model of augmentation cystoplasty. Biomaterials. 2013; 34:8681–9. [PubMed: 23953839]
24. Seth A, Chung YG, Gil ES, Tu D, Franck D, Di Vizio D, et al. The performance of silk scaffolds in a rat model of augmentation cystoplasty. Biomaterials. 2013; 34:4758–65. [PubMed: 23545287]
25. Kim UJ, Park J, Kim HJ, Wada M, Kaplan DL. Three-dimensional aqueous-derived biomaterial scaffolds from silk fibroin. Biomaterials. 2005; 26:2775–85. [PubMed: 15585282]
26. Seth A, Chung YG, Kim D, Ramachandran A, Cristofaro V, Gomez P 3rd, et al. The impact of discrete modes of spinal cord injury on bladder muscle contractility. BMC Urol. 2013; 13:24. [PubMed: 23668225]

27. Tu DD, Seth A, Gil ES, Kaplan DL, Mauney JR, Estrada CR Jr. Evaluation of biomaterials for bladder augmentation using cystometric analyses in various rodent models. J Vis Exp. 2012; 66:3981. [PubMed: 22907252]

28. Chung YG, Tu D, Franck D, Gil ES, Algarrahi K, Adam RM, et al. Acellular bi-layer silk fibroin scaffolds support tissue regeneration in a rabbit model of onlay urethroplasty. PLoS One. 2014; 9:e91592. [PubMed: 24632740]

29. Kruse MN, Bray LA, De Groat WC. Influence of spinal cord injury on the morphology of bladder afferent and efferent neurons. J Auton Nerv Syst. 1995; 54:215–24. [PubMed: 7490423]

30. Kropp BP, Eppley BL, Prevel CD, Rippy MK, Harruff RC, Badylak SF, et al. Experimental assessment of small intestinal submucosa as a bladder wall substitute. Urology. 1995; 46:396–400. [PubMed: 7660517]

31. Vaught JD, Kropp BP, Sawyer BD, Rippy MK, Badylak SF, Shannon HE, et al. Detrusor regeneration in the rat using porcine small intestinal submucosal grafts: functional innervation and receptor expression. J Urol. 1996; 155:374–8. [PubMed: 7490890]

32. Shang K, Rnjak-Kovacina J, Lin Y, Hayden RS, Tao H, Kaplan DL. Accelerated in vitro degradation of optically clear low beta-sheet silk films by enzyme-mediated pretreatment. Trans Vis Sci Tech. 2013; 2:2.

33. Sharma AK, Bury MI, Fuller NJ, Marks AJ, Kollhoff DM, Rao MV, et al. Cotransplantation with specific populations of spina bifida bone marrow stem/progenitor cells enhances urinary bladder regeneration. Proc Natl Acad Sci U S A. 2013; 110:4003–8. [PubMed: 23431178]

34. Critser, PJ.; Yoder, MC. Biophysical properties of scaffolds modulate human blood vessel formation from circulating endothelial colony-forming cells. In: Gerecht, S., editor. Biophysical regulation of vascular differentiation and assembly. New York: Springer; 2011. p. 89-110.

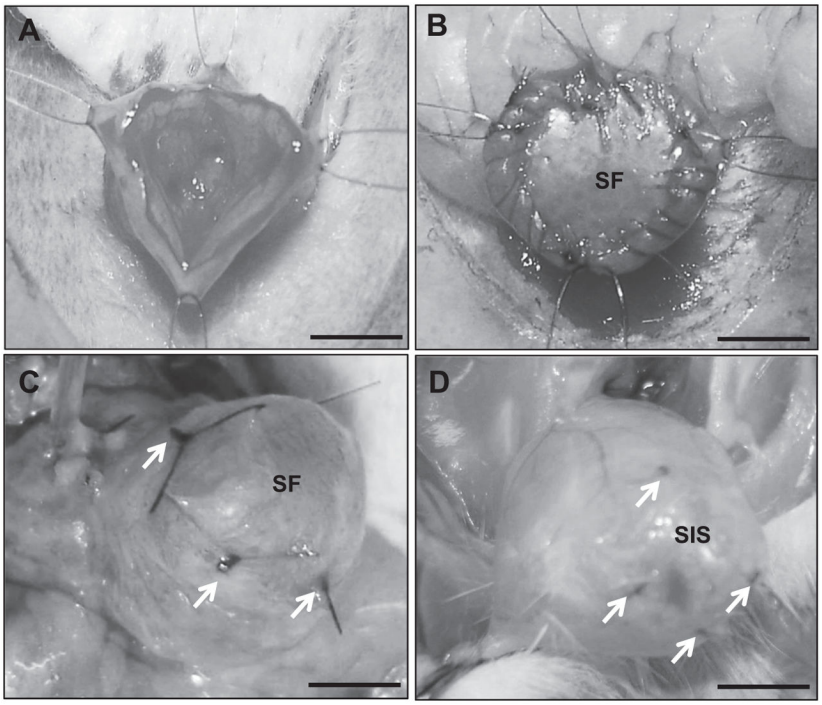

Fig. 1.

Rat bladder augmentation model. Photomicrographs of various surgical stages of scaffold implantation and gross morphology of regenerated tissues. [A] Cystotomy and exposure of the bladder lumen. [B] Anastomosis of bi-layer silk fibroin (SF) graft into the bladder defect. [C, D] Regenerated tissues present within the original implantation sites supported by bi-layer SF scaffolds [C] and small intestinal submucosa (SIS) matrices [D]. Arrows denote original marking sutures. Scale bars = 3 mm.

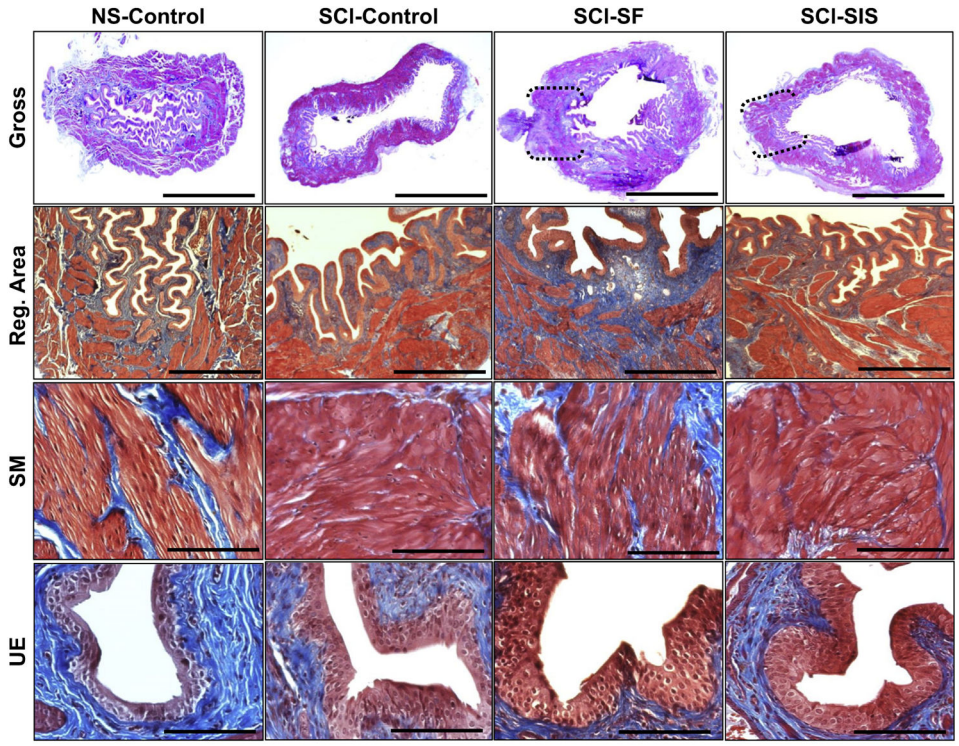

Fig. 2.

Histological evaluations (MTS analysis) of bladder tissue morphology in control and implant groups. [1st row] Photomicrographs of gross bladder cross-sections of each matrix group following 10 wk of implantation as well as non-augmented controls. Brackets represent sites of original scaffold implantation as determined by the presence of marking sutures. Scale bars = 2.5 mm. [2nd row] Magnification of global tissue regeneration bracketed in 1st row in scaffold groups and representative tissue architecture in non-augmented controls. Scale bars = 600 μm. [3rd and 4th rows] Magnified smooth muscle (SM) bundles and urothelium (UE) displayed in 2nd row. Scale bars = 200 μm.

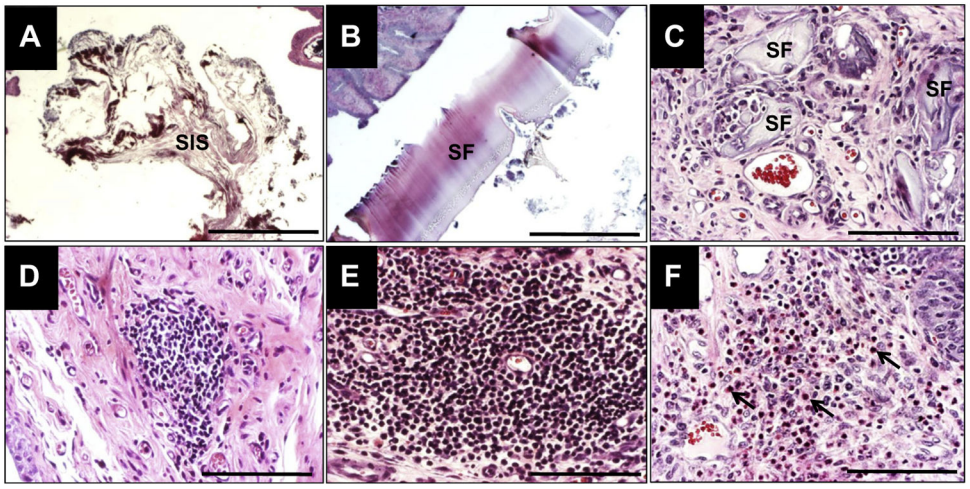

Fig. 3.

Extent of biomaterial degradation and inflammatory responses elicited by scaffold groups. [A–C] Photomicrographs of H&E-stained, residual fragments of SIS [A] and bi-layer SF matrices [B] present in the bladder lumen and regenerated bladder wall [C] at 10 wk post-op. [A, B], scale bars = 600 μm; [C], scale bar = 200 μm. [D–F] Photomicrographs of chronic and acute inflammatory reactions in the *de novo* bladder wall (H&E-stained) supported by SIS [D] and bi-layer SF [E, F] scaffolds at 10 wk following implantation. [D, E] Mobilized follicular aggregates of mononuclear cell infiltrates indicative of chronic inflammation. [F] Arrows denote eosinophil granulocytes representing an acute inflammation response. [D–F], scale bars = 200 μm.

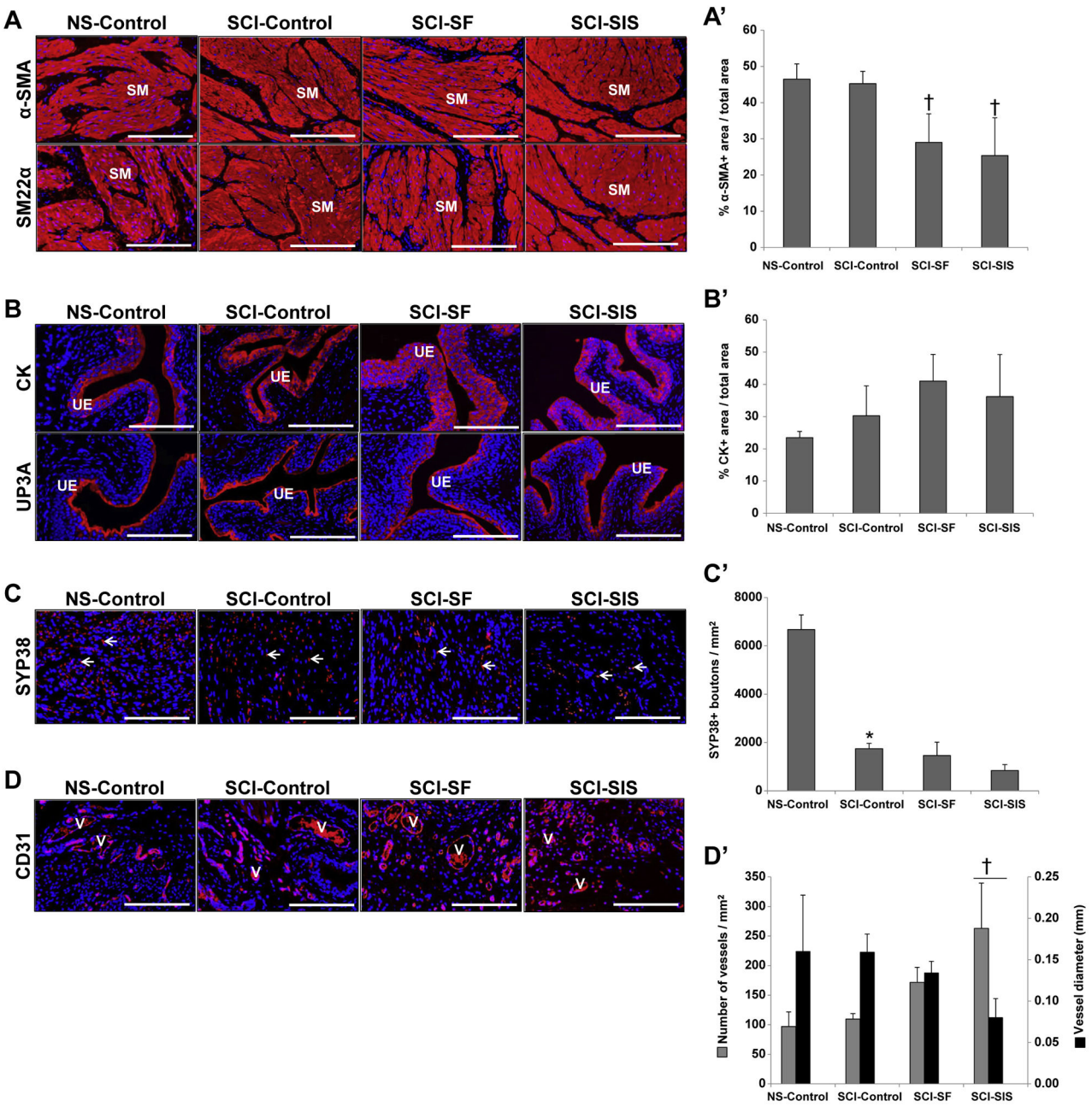

Fig. 4.

Immunohistochemical and histomorphometric assessments of bladder tissue morphology in control and biomaterial groups. [A–D] Photomicrographs protein expression of smooth muscle (SM) contractile markers (α-SMA and SM22α); urothelial (UE)-associated uroplakin (UP) 3A and cytokeratins (CK); the innervation marker, synaptophysin (SYP38); and the endothelial maker CD31 in non-augmented control tissues and sites of tissue repair supported by scaffold groups. V denotes CD31+ vessels and arrows represent SYP38+ boutons. For all panels, respective marker expression is displayed in red (Cy3 labeling) and blue denotes DAPI nuclear counterstain. Scale bars in all panels = 200 μm. [A′–D′] Histomorphometric analysis of the extent of regenerated α-SMA+ SM bundles [A′], CK+

urothelium [B′], SYP38+ boutons [C′], CD31+ vessels present in non-augmented control groups and in sites of tissue repair mediated by implant groups at 10 wk post-op. (*) = $p < 0.05$ in comparison to NS-control. (†) = $p < 0.05$ in comparison to SCI-control.

Table 1

Cystometric analysis of experimental groups. Comparisons of urodynamic parameters in non-augmented control cohorts and implant groups following 10 wk post-op. (*) = $p < 0.05$ in comparison to NS-control. (†) = $p < 0.05$ in comparison to SCI-control.

Urodynamic parameters	NS-control	SCI-control	SCI–SF	SCI–SIS
Capacity (ml)	1.581 ± 0.58	4.90 ± 1.91	2.95 ± 2.71	3.74 ± 3.00
Compliance (ml/cm H_2O)	1.89 ± 4.48	0.89 ± 1.59	1.56 ± 2.11	1.73 ± 1.70
Start filling pressure (cm H_2O)	6.36 ± 5.42	18.72 ± 12.91*	14.44 ± 3.27	10.00 ± 7.49†
End filling pressure (cm H_2O)	11.73 ± 6.81	29.20 ± 17.70*	18.58 ± 4.73	14.52 ± 13.39†
Peak intravesical pressure (cm H_2O)	30.26 ± 10.72	77.13 ± 36.44*	40.08 ± 8.61†	44.11 ± 10.93†
Resting pressure (cm H_2O)	5.28 ± 6.08	16.85 ± 12.54*	13.59 ± 3.36	8.48 ± 7.87†
Voided volume (ml)	1.22 ± 0.61	1.11 ± 0.70	1.55 ± 1.00	1.47 ± 0.84
Post void residual volume (ml)	0.30 ± 0.26	4.01 ± 1.72*	1.57 ± 1.64	2.82 ± 3.10
SNVC	0.71 ± 0.75	11.60 ± 13.74*	5.25 ± 10.79	9.81 ± 12.48